Latypova, Renata; Nyo, Tun Tun; Seppälä, Oskari; Fangnon, Eric; Yagodzinskyy, Yuriy; Mehtonen, Saara; Hänninen, Hannu; Kömi, Jukka; Pallaspuro, Sakari

Effect of prior austenite grain morphology on hydrogen embrittlement behaviour under plastic straining in as-quenched 500 HBW steels

Published in:
23rd European Conference on Fracture, ECF 2022

DOI:
10.1016/j.prostr.2022.12.110

Published: 01/01/2022

Document Version
Publisher's PDF, also known as Version of record

Please cite the original version:
Latypova, R., Nyo, T. T., Seppälä, O., Fangnon, E., Yagodzinskyy, Y., Mehtonen, S., Hänninen, H., Kömi, J., & Pallaspuro, S. (2022). Effect of prior austenite grain morphology on hydrogen embrittlement behaviour under plastic straining in as-quenched 500 HBW steels. In P. Moreira, & L. Reis (Eds.), *23rd European Conference on Fracture, ECF 2022* (pp. 871-878). (Procedia Structural Integrity; Vol. 42). Elsevier. https://doi.org/10.1016/j.prostr.2022.12.110

Available online at www.sciencedirect.com

ScienceDirect

Procedia Structural Integrity 42 (2022) 871–878

Structural Integrity Procedia

www.elsevier.com/locate/procedia

23 European Conference on Fracture - ECF23

Effect of prior austenite grain morphology on hydrogen embrittlement behaviour under plastic straining in as-quenched 500 HBW steels

Renata Latypova[a,]*, Tun Tun Nyo[a], Oskari Seppälä[a], Eric Fangnon[b], Yuriy Yagodzinskyy[b], Saara Mehtonen[c], Hannu Hänninen[b], Jukka Kömi[a], Sakari Pallaspuro[a]

[a]*Materials and Mechanical Engineering, Centre for Advanced Steels Research, University of Oulu, Finland*
[b]*Department of Mechanical Engineering, School of Engineering, Aalto University, 02150 Espoo, Finland*
[c]*SSAB, 92100 Raahe, Finland*

Abstract

Prior austenite grain (PAG) structure is an important factor influencing hydrogen embrittlement (HE) susceptibility of ultrahigh-strength steels. In this study, the effect of PAG shape and size on HE behaviour is investigated using a novel tuning-fork testing method and hydrogen thermal desorption spectroscopy (TDS). Different PAG structures were acquired via re-austenitization (860 °C = A860, 960 °C = A960) and rapid quenching of an as-received 500 HBW direct-quenched (DQ) steel, which has an auto-tempered lath-martensitic microstructure and elongated PAG morphology. Fractography reveals different crack propagation mechanisms depending on the PAG shape. With the elongated PAG structure, hydrogen-induced crack propagation transverse to elongated PAGs was transgranular quasi-cleavage. Propagation was partially intergranular with the equiaxed PAG structures, regardless of the PAG size, leading to equally faster fracture. The TDS results show that there are no significant differences between the total hydrogen contents, but re-austenitized A860 and A960 steels contain a higher fraction of weakly trapped hydrogen. This indicates that the PAG boundaries are not the dominant hydrogen traps, and the different crack propagation mechanisms are rather linked to the geometrical shape of the grain structure.

Keywords: steel; hydrogen embrittlement; prior austenite grain structure; tuning-fork test; TDS

10.1016/j.prostr.2022.12.110

1. Introduction

Hydrogen embrittlement (HE) is a known issue for ultrahigh-strength steels, where the presence of hydrogen in the material causes unwanted brittleness and degradation of mechanical properties. [1] Hydrogen (H) is the lightest of elements, and it can readily diffuse inside the material interstitially, along the grain boundaries and moving dislocations. [2,3] In HE failures, hydrogen diffuses to the regions of high tensile stresses, and with a critical concentration causes fracture. [4] However, hydrogen diffusion is hindered by various traps present in the microstructure. [4,5] The traps can be divided into weak reversible and strong irreversible traps. In weak traps that have a low binding energy, hydrogen is released easily, which can promote HE. The strong traps have a high binding energy, immobilising hydrogen, which may improve the HE resistance if the traps are distributed evenly. [6,7]

Martensitic ultrahigh-strength steels are especially prone to HE. [8] Martensite formation occurs by quenching of austenite, where each prior austenite grain (PAG) transforms into martensite consisting of laths, blocks, and packets. All above-mentioned interfaces are possible hydrogen trapping sites together with dislocations, vacancies, solutes, precipitates, inclusions, and voids. [6] Martensitic microstructure inherits the shape and size of the PAG structure, which affect the properties of a steel, like HE susceptibility as PAG boundaries can act as diffusion paths or hydrogen traps. [9,10] In hydrogen-induced fracture, cracks often propagate along the PAG boundaries causing brittle intergranular fracture. [11]

The shape and size of the PAG structure can be modified by manufacturing processes and parameters such as austenitization temperature and finishing rolling temperature. [12,13] Traditionally manufactured martensitic steels have an equiaxed PAG structure as a result of the reheating and quenching process, where austenite is always recrystallized before quenching. [14] A modern way to produce martensitic steels is direct quenching (DQ), where hot rolling can be done with either recrystallized or non-recrystallized austenite, followed by immediate quenching. If hot rolling is done below the recrystallization finish temperature, the PAG structure will be elongated parallel to the rolling direction. [15,16] In this study, we investigate the HE susceptibility of elongated and equiaxed PAG structures from the same alloy.

2. Materials and methods

2.1. Test materials

A direct-quenched (DQ) martensitic steel 0.25C-0.1Si-0.25Mn (wt.%) with elongated PAG structure was re-austenitized at 860°C/960°C for 25 min and quenched in a water-oil emulsion. As a result, two steels (A860 and A960) with different equiaxed PAG structures were obtained with the same alloying composition and similar hardness and tensile strength as those of the original DQ material. All steels have an auto-tempered martensitic microstructure with a negligible amount of retained austenite (< 1%) estimated by XRD analysis. The studied PAG structures are presented in

Figure 1, and Table 1 shows the mechanical properties, average PAG size (d_G), PAG boundary surface area per unit volume (S_V), and PAG aspect ratio (RD/ND) of each steel grade, where RD = rolling direction and ND = normal direction. DQ and A860 steels have approximately the same d_G, but different PAG shapes and A860 and A960 steels have the same PAG shape but a fourfold difference in d_G. This type of steel comparison allows for investigating the effect of both the size and shape of the PAG structure.

Table 1. Mechanical properties and PAG characteristics of investigated steels.

Material	Measured hardness (HBW)	Yield strength = YS (MPa)	Tensile strength = TS (MPa)	d_G (μm)	S_V (mm^2/mm^3)	RD/ND
DQ	484 (± 3)	1411	1632	9.6	270	3
A860	482 (± 2)	1155	1592	9.4	221	1
A960	475 (± 2)	1102	1529	42.6	46	1

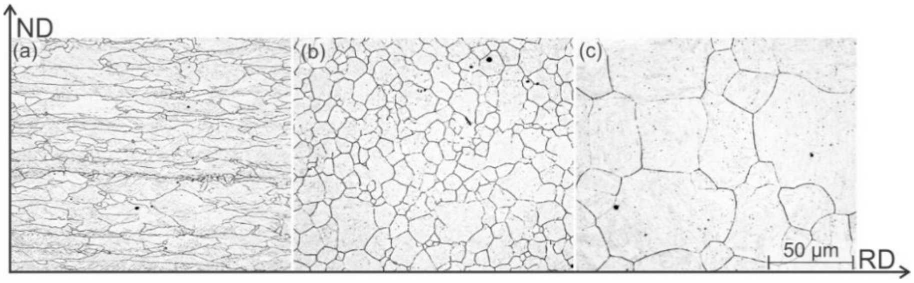

Figure 1. PAG structures of (a) the original DQ, and re-austenitized (b) A860 and (c) A960 steels.

2.2. Testing methods

Novel tuning-fork test and hydrogen thermal desorption spectroscopy (TDS) were utilized in this study. In the tuning-fork test, notched specimens were locally stressed beyond the yield point and in situ charged until failure (3% NaCl + 3 g/l NH_4SCN, -1.2 $V_{Hg/Hg2SO4}$). Tuning-fork specimens were cut by wire electrical discharge machining (WEDM) and all the outer specimen surfaces were lightly polished with 600 and 1200 grit emery papers. Stressing of the specimens was conducted with a loadcell clamping (HBM C9C, 2 kN) that applied arm displacement of 5.3 – 5.7 mm. In the selected environment, testing of unnotched and notched specimens was not possible in the elastic region. Even when stressed at the yield point of the material, the stress concentration was ineffective in causing crack initiation within 24 hours.

During hydrogen charging, a crack initiates at the bottom of the notch under tensile stress state and propagates through the specimen. Figure 2a presents the tuning-fork geometry with marked rolling direction (RD) and Figure 2b the clamped specimen with the highlighted plastic zone. Our previous research has shown that steels with equiaxed PAG structures produce similar results with differently oriented specimens [30]. Therefore, RD was only considered with DQ specimens due to the microstructural anisotropy of the PAG structure.

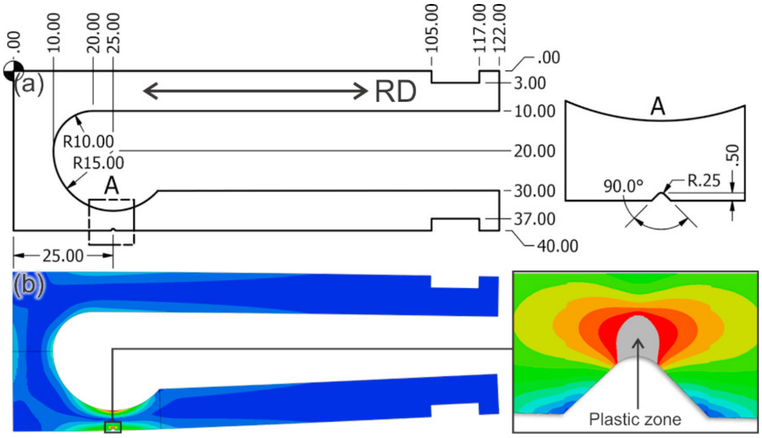

Figure 2. (a) Tuning-fork geometry with marked RD and (b) FEM model of stressed tuning-fork with a small plastic region.

The obtained time-force data from each test was used to calculate the crack initiation time (ti) and time-to-fracture (tf) with a specially designed graphical user interface (GUI) tool. First, a moving point average of 5 was applied. Then, based on the average of the first 100 values, and the average of the last 20 values, the respective start and end lines were drawn. The angle between the start/end line and the data points was compared, and when it reached 5°, it was marked as ti/tf as presented in Figure 3.

.

To compare the different materials, finite element method (FEM) models were calculated according to the applied distance to quantify the maximum opening stress component (σ_{11}) for each steel. The data was then normalised by dividing each t_i and t_f by material specific σ_{11}/YS to allow the comparison of materials with different yield strengths.

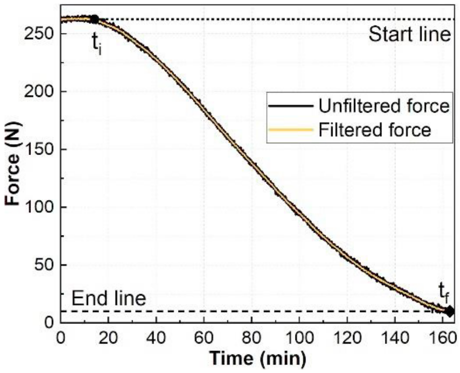

Figure 3. An example of a t-F curve with initiation time (t_i) and time-to-fracture (t_f) determined with the 5° limiting angle.

The same hydrogen charging conditions as in the tuning-fork tests were utilized in 2.5 h charging of TDS specimens (3 samples/material). For the selection of hydrogen charging time, hydrogen uptake was measured as a function of the electrochemical charging time for DQ in the range of 0.5 – 14 h.

TDS specimens (10 x 5 x 1 mm) were wire cut by EDM and mechanically polished with 1200 grit emery paper to remove the oxidised layer. Each specimen was spot welded to an electrode extender and the welded section was Teflon taped to expose only the specimen surface to the electrolyte. After charging, the specimens were de-coupled from the extender, cleaned with running distilled water, and sent for hydrogen concentration measurement. Before TDS, the specimens were dried with helium to prevent formation of moisture on surfaces. The time after H-charging to the initiation of TDS measurements did not exceed 10 minutes.

3. Results and discussion

3.1. Tuning-fork test

Normalised force-time data from the tuning-fork tests with steels DQ, A860, and A960 are presented in Figure 4. All curves have a similar shape, with an initial steady-state initiation region followed by a gradual lowering of the force values caused by crack propagation.

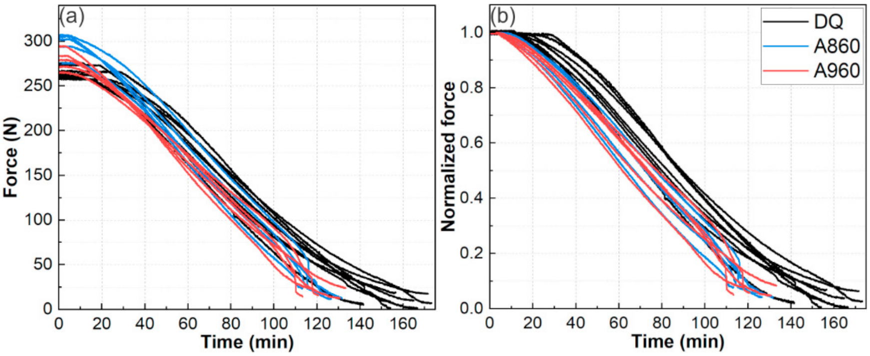

Figure 4. (a) Raw and (b) normalised t-F data from tuning-fork tests.

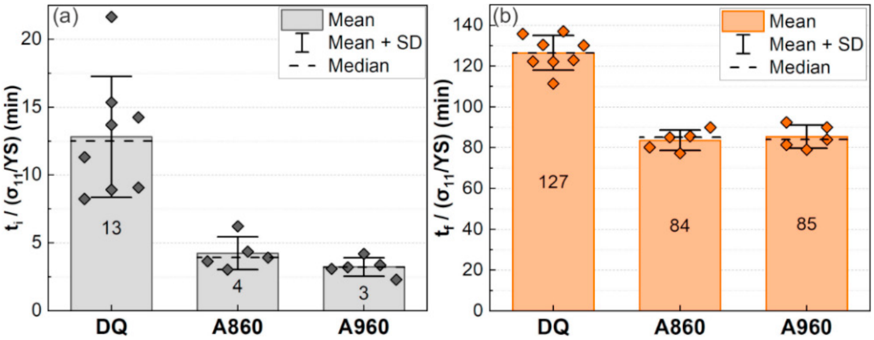

Figure 5. Normalised initiation time (ti) and time-to-fracture (tf) results of investigated materials.

Figure 5 shows normalised t_i and t_f results. Both t_i and t_f times are significantly longer ($p = 0.05$) for the elongated PAG structure in comparison to the equiaxed PAG structures, which suggests that the elongated PAG structure has a better resistance against HE. At the same time, different grain sizes of the equiaxed PAG structures show similar performance levels, indicating that the PAG size in the range of 10 – 40 µm does not affect HE susceptibility. It must be noted that the results followed the same trend regardless of normalisation of t_i and t_f. The same trend for t_i persists also with calculated hydrostatic stress, which is the driving force for H diffusion.

Fractography reveals different crack propagation mechanisms depending on the PAG shape and/or heat treatment (Figure 6). Hydrogen-induced crack propagation is transgranular quasi-cleavage with the elongated PAG structure, and with the equiaxed PAG structures, it is partly intergranular.

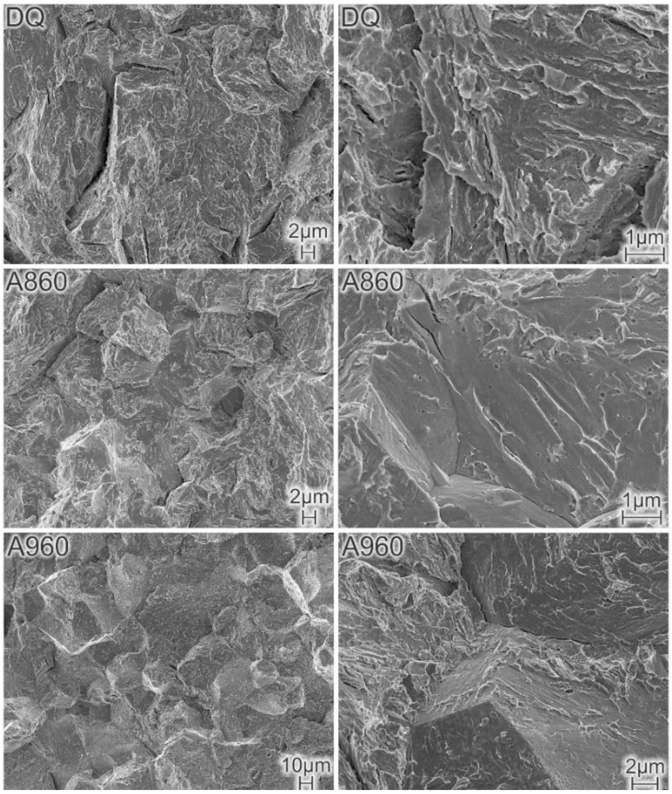

Figure 6. General (left) and detailed (right) views of fracture surfaces of investigated steels.

Because of the differing crack paths, shorter t_f can be linked to the intergranular crack propagation of A860 and A960 steels regardless of the PAG size. Intergranular cracking appears often in reheated and quenched martensitic steels in hydrogen-related fracture. This tendency increases with increasing segregation of impurities and second-phase particles along the PAG boundaries. [17] There is a different thermomechanical history for DQ with strained austenite and A860/A960 steels with unstrained austenite. With high temperature austenitization of A860/A960, impurities can locally accumulate at the PAG boundaries in strain-free austenite. However, in this case, the amount of grain boundary impurity elements is globally the same for all steels. In theory, a bigger S_V of A860 provides enhanced distribution of impurity elements over a larger area in comparison to A960. This should improve the hydrogen resistance, but it did not have an effect. Therefore, the change in the cracking mechanisms is mainly a consequence of different PAG shapes, and likely also of differing heat and deformation histories.

With the elongated PAG boundaries, the dihedral angle in the transverse direction is larger in comparison to the equiaxed structure. Therefore, intergranular crack propagation in the elongated PAG structure requires more deflections and energy to occur in comparison to the equiaxed PAG structure. [18] If the applied stress is parallel to the elongated PAGs, transgranular quasi-cleavage facture occurs since large stresses do not act on the PAG boundaries. [19] With an elongated, irregular PAG shape, the structure of grain boundaries is considered to suppress intergranular crack propagation to a certain degree, but the equiaxed PAG structure is more prone to the intergranular crack propagation.

3.2. TDS

For DQ, hydrogen uptake is measured as a function of electrochemical charging time as presented in Figure 7. After 2.5 h, hydrogen concentration approaches a certain plateau, and therefore this time is enough to provide saturated hydrogen concentration and a homogeneous distribution of hydrogen in the specimens.

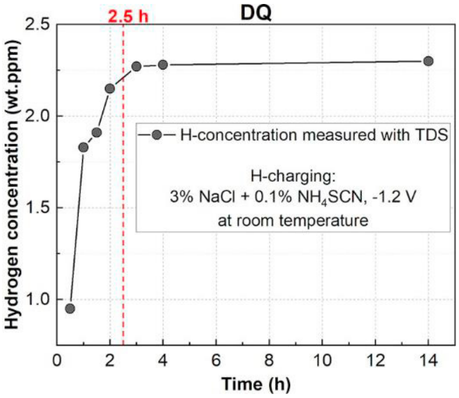

Figure 7. Time-dependent hydrogen uptake of DQ.

The TDS curves and calculated total hydrogen contents are presented in Figure . The hydrogen desorption curves consist of two distinctive components, a lower temperature peak (375 – 500 K), and a higher temperature peak (500 – 875 K). The lower temperature peak is typically associated with weakly trapped hydrogen in traps such as grain boundaries and dislocations and high-temperature peak with irreversible trapping sites. [20,21]

No significant differences are detected between the total hydrogen contents, which is contradictory because of the fourfold difference in PAG size between DQ/A860 and A960 steels. The effect of PAG size on hydrogen concentration has been previously investigated with a tempered martensitic steel, where different equiaxed PAG sizes were obtained by varying re-austenitization temperature in the range of 880 – 1250 °C. Hydrogen content was reported to be 0.3 wt.ppm for an average PAG size of 36 μm, which was less than half for the same alloy steel with a PAG size of 6 μm. [13] In 8Ni-0.1C martensitic steel, PAG refinement from 24 μm to 4.2 μm increased the hydrogen absorption capacity, too. [22] However, these studies do not mention the amount of retained austenite, which can substantially affect hydrogen content, while in our case the amount of retained austenite was less than 1 % for all materials.

Despite the similar total hydrogen content, there are distinct differences between the lower temperature TDS peaks of the investigated steels. For A860 and A960 steels, the lower temperature TDS peaks are significantly higher in comparison to that of DQ, suggesting that these steels contain more weakly trapped hydrogen. This contrasts also with the S_V of the materials since the steel with a lower amount of PAG boundaries contains more weakly trapped hydrogen. Further investigations are required to understand the true state of hydrogen and the mechanisms governing the hydrogen-microstructure interaction, diffusivity and trapping in the studied steels. Current results indicate that the PAG boundaries are not the dominant weak hydrogen traps, and the different crack propagation is rather linked to the geometrical shape of the grain structure and grain growth mechanisms.

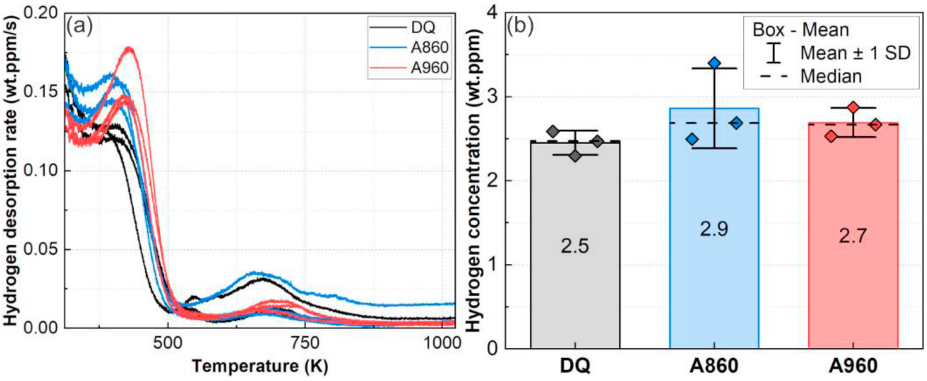

Figure 8. (a) TDS curves and (b) total hydrogen content of investigated steels.

4. Conclusions

The effect of different PAG structures of the same alloy on hydrogen embrittlement (HE) susceptibility was investigated with a novel tuning-fork test under plastic straining and complemented with thermal desorption spectroscopy (TDS) measurements using the same hydrogen charging environment. DQ steel with elongated PAG structure has a superior HE resistance in transverse direction, with longer crack initiation time and time-to-fracture in comparison to re-austenitized steels with equiaxed PAG structures. Differences are attributed to a change in the crack propagation mechanism from transgranular quasi-cleavage to partly intergranular fracture, depending on the PAG shape. Elongated PAG structure leads to a slower quasi-cleavage fracture, and equiaxed PAG structure is prone to intergranular crack propagation. TDS results show that investigated steels have similar total hydrogen concentrations but different trapping properties with equiaxed recrystallized PAG structures having more weakly trapped hydrogen. The results indicate that PAG boundaries are not the dominant hydrogen traps in these as-quenched martensitic steels, and the different crack propagation modes are linked rather to the geometrical shape of the grain structure and grain growth mechanisms.

Acknowledgements

This research was supported by Business Finland Oy and Academy of Finland (#337108). The projects ISA – Intelligent Steel Applications and FOSSA– Fossil-Free Steel Applications, are acknowledged. The authors wish to thank the technical staff of the Materials and Mechanical Engineering unit at the University of Oulu for their help with experimental work and sample preparation.

References

[1] J. Woodtli, R. Kieselbach, Damage due to hydrogen embrittlement and stress corrosion cracking, Eng. Fail. Anal. 7 (2000) 427–450. https://doi.org/10.1016/S1350-6307(99)00033-3.

[2] D. Rudomilova, T. Prošek, P. Salvetr, A. Knaislová, P. Novák, R. Kodým, G. Schimo-Aichhorn, A. Muhr, H. Duchaczek, G.

Luckeneder, The effect of microstructure on hydrogen permeability of high strength steels, Mater. Corros. 71 (2020) 909–917. https://doi.org/10.1002/maco.201911357.

[3] D. Mallick, N. Mary, V.S. Raja, B. Normand, Study of Diffusible Behavior of Hydrogen in First Generation Advanced High Strength Steels, Metals (Basel). 11 (2021) 782. https://doi.org/10.3390/met11050782.

[4] J. Venezuela, Q. Liu, M. Zhang, Q. Zhou, A. Atrens, A review of hydrogen embrittlement of martensitic advanced high-strength steels, Corros. Rev. 34 (2016) 153–186. https://doi.org/10.1515/corrrev-2016-0006.

[5] Q. Liu, A. Atrens, Reversible hydrogen trapping in a 3.5NiCrMoV medium strength steel, Corros. Sci. 96 (2015) 112–120. https://doi.org/10.1016/j.corsci.2015.04.011.

[6] J. Venezuela, Q. Zhou, Q. Liu, M. Zhang, A. Atrens, Hydrogen Trapping in Some Automotive Martensitic Advanced High-Strength Steels, Adv. Eng. Mater. 20 (2018) 1700468. https://doi.org/10.1002/adem.201700468.

[7] H.K.D.H. Bhadeshia, Prevention of hydrogen embrittlement in steels, ISIJ Int. 56 (2016) 24–36. https://doi.org/10.2355/isijinternational.ISIJINT-2015-430.

[8] S.K. Dwivedi, M. Vishwakarma, Hydrogen embrittlement in different materials: A review, Int. J. Hydrogen Energy. 43 (2018) 21603–21616. https://doi.org/10.1016/j.ijhydene.2018.09.201.

[9] G. Krauss, Martensitic Structure, in: Encycl. Iron, Steel, Their Alloy., CRC Press, 2016: pp. 2182–2187. https://doi.org/10.1081/E-EISA-120049074.

[10] A. Shibata, H. Takahashi, N. Tsuji, Microstructural and crystallographic features of hydrogen related crack propagation in low carbon martensitic steel, ISIJ Int. 52 (2012) 208–212. https://doi.org/10.2355/isijinternational.52.208.

[11] G. Krauss, Deformation and fracture in martensitic carbon steels tempered at low temperatures, Metall. Mater. Trans. B. 32 (2001) 205–221. https://doi.org/10.1007/s11663-001-0044-4.

[12] A.J. Kaijalainen, P.P. Suikkanen, T.J. Limnell, L.P. Karjalainen, J.I. Kömi, D.A. Porter, Effect of austenite grain structure on the strength and toughness of direct-quenched martensite, J. Alloys Compd. 577 (2013) S642–S648. https://doi.org/10.1016/j.jallcom.2012.03.030.

[13] Y. Liu, M. Wang, G. Liu, Hydrogen trapping in high strength martensitic steel after austenitized at different temperatures, Int. J. Hydrogen Energy. 38 (2013) 14364–14368. https://doi.org/10.1016/j.ijhydene.2013.08.121.

[14] H. Bhadeshia, R. Honeycombe, Steels Microstructure and Properties, 3rd ed., Elsevier, Oxford, United Kingdom, 2006. https://doi.org/10.1016/B978-0-7506-8084-4.X5000-6.

[15] J. Kömi, P. Karjalainen, D. Porter, Direct-Quenched Structural Steels, in: Encycl. Iron, Steel, Their Alloy., CRC Press, 2016: pp. 1109–1125. https://doi.org/10.1081/E-EISA-120049737.

[16] A. Kaijalainen, Effect of microstructure on the mechanical properties and bendability of direct-quenched ultrahigh-strength steels, Acta Universitatis Ouluensis C582, 2016.

[17] M. Nagumo, H. Matsuda, Function of hydrogen in intergranular fracture of martensitic steels, Philos. Mag. A. 82 (2002) 3415–3425. https://doi.org/10.1080/01418610208240452.

[18] Y. Nie, Y. Kimura, T. Inoue, F. Yin, E. Akiyama, K. Tsuzaki, Hydrogen Embrittlement of a 1500-MPa Tensile Strength Level Steel with an Ultrafine Elongated Grain Structure, Metall. Mater. Trans. A. 43 (2012) 1670–1687. https://doi.org/10.1007/s11661-011-0974-7.

[19] S. Yamasaki, T. Tarui, M. Kubota, Evaluation method for delayed fracture susceptibility of steels and development of high tensile strength steels with high delayed fracture resistance, Nippon Steel Tech. Rep. (1999) 50–55.

[20] E. Fangnon, Y. Yagodzinskyy, E. Malictki, S. Mehtonen, E. Virolainen, P. Vilaça, Determination of critical hydrogen concentration and its effect on mechanical performance of 2200 mpa and 600 hbw martensitic ultra-high-strength steel, Metals (Basel). 11 (2021). https://doi.org/10.3390/met11060984.

[21] M. Koyama, M. Rohwerder, C.C. Tasan, A. Bashir, E. Akiyama, K. Takai, D. Raabe, K. Tsuzaki, Recent progress in microstructural hydrogen mapping in steels: quantification, kinetic analysis, and multi-scale characterisation, Mater. Sci. Technol. (United Kingdom). 33 (2017) 1481–1496. https://doi.org/10.1080/02670836.2017.1299276.

[22] H. Fuchigami, H. Minami, M. Nagumo, Effect of grain size on the susceptibility of martensitic steel to hydrogen-related failure, Philos. Mag. Lett. 86 (2006) 21–29. https://doi.org/10.1080/09500830500482316.